



RESEARCH ARTICLE

10.1002/2014GC005320

Evidence of an upper mantle seismic anomaly opposing the Cocos slab beneath the Isthmus of Tehuantepec, Mexico

YoungHee Kim¹, Hobin Lim¹, Meghan S. Miller², Fred Pearce³, and Robert W. Clayton⁴

Key Points:

- Imaged two opposing seismic structures beneath southern Mexico
- Explained anomalous upper plate deformation features based on our image
- Identified anomalous intermediate-depth earthquake activities

Correspondence to:

Y.H. Kim,
youngheekim@snu.ac.kr

Citation:

Kim, Y.H., H. Lim, M. S. Miller, F. Pearce, and R. W. Clayton (2014), Evidence of an upper mantle seismic anomaly opposing the Cocos slab beneath the Isthmus of Tehuantepec, Mexico, *Geochem. Geophys. Geosyst.*, 15, 3021–3034, doi:10.1002/2014GC005320.

Received 27 FEB 2014

Accepted 5 JUL 2014

Accepted article online 10 JUL 2014

Published online 25 JUL 2014

¹School of Earth and Environmental Sciences, Seoul National University, Seoul, South Korea, ²Department of Earth Sciences, University of Southern California, Los Angeles, California, USA, ³Department of Earth, Atmospheric and Planetary Sciences, Massachusetts Institute of Technology, Cambridge, Massachusetts, USA, ⁴Seismological Laboratory, California Institute of Technology, Pasadena, California, USA

Abstract Subduction of the Cocos plate beneath southern Mexico is characterized by several unusual features, such as a discontinuous volcanic arc, unusual arc chemistry, and anomalously low topography of Tehuantepec Isthmus. Recent seismic images from both receiver functions and seismic tomography suggest that there may be an additional, opposing structure dipping to the southwest from the Gulf of Mexico, and these images have been previously explained by a southwest-dipping slab. However, standard models of the Caribbean tectonic history do not support this interpretation. To better define the Cocos slab's structure and the possible existence of a structure dipping in the opposite direction, dense seismic data across southern Mexico are used to form high-resolution seismic images, based on the 2-D generalized radon transform method, and to relocate regional earthquakes. Our images show the Cocos plate dipping at 30° to the northeast encounters the anomaly that is dipping in the opposite sense at ~150 km depth. Relocated seismicity clearly delineates a Wadati-Benioff zone that marks the subducting Cocos plate. A cluster of seismicity also appears at ~150 km depth which may be related to the subduction of the Tehuantepec ridge and/or to the imaged seismic structure with opposite polarity.

1. Introduction

There are a number of anomalous tectonic features in southern Mexico that are assumed to be a result of subduction, but are not well-explained by a simple model of the Cocos plate subducting underneath the North American plate to the northeast. Recent receiver function and tomography images based on the Veracruz-Oaxaca (VEOX) seismic line (Figure 1, black squares) [Veracruz-Oaxaca (VEOX), 2010] both show an enigmatic seismic structure, which dips in an opposite direction to the Cocos slab [Kim *et al.*, 2011; Chen and Clayton, 2012] beneath the northern extent of the VEOX line. We exploit the same densely spaced seismic data [VEOX, 2010] by using the 2-D generalized radon transform method [Bostock *et al.*, 2001, and references therein] and relocating regional seismicity [Waldhauser and Ellsworth, 2000] to better define this velocity structure and the subducting Cocos slab beneath southern Mexico. Here we introduce a number of tectonic and volcanic features that may be related to this unusual seismic structure.

1.1. Subduction Geometry and Volcanic Arc Locations

The subduction of the Cocos plate along the Middle America Trench is defined by a steep-shallow-steep progression of slab dip angles despite the monotonic southeastward increase in the plate velocity and age along the trench from ~104.5°W to 95°W (Figure 1). Near the Rivera plate junction at 104.5°W, the Cocos plate is ~11 Ma old, is converging at 4.8 cm/yr and has a dip of ~50° [DeMets and Stein, 1990; Pardo and Suarez, 1995]. Near the Tehuantepec ridge (at ~95°W), the plate is slightly older (23 Ma) and is converging at 7.1 cm/yr and dipping into the mantle at ~30° [DeMets and Stein, 1990; Pardo and Suarez, 1995]. The middle of the plate is subducting nearly horizontally [Perez-Campos *et al.*, 2008; Kim *et al.*, 2010, 2012b] as imaged by the Meso-America Subduction Experiment (MASE) [Meso-America Subduction Experiment (MASE), 2007] transect shown in Figure 1a (white circles). Previous results also show that the slab dip of the Cocos plate beneath southern Mexico is ~30° based on relocated seismicity [Pardo and Suarez, 1995], and, more recently, ~25–26° based on teleseismic receiver function analysis (see Figure 2a, slab contours) [Melgar and Perez-Campos, 2010; Kim *et al.*, 2011] using a dense array data set [VEOX, 2010].

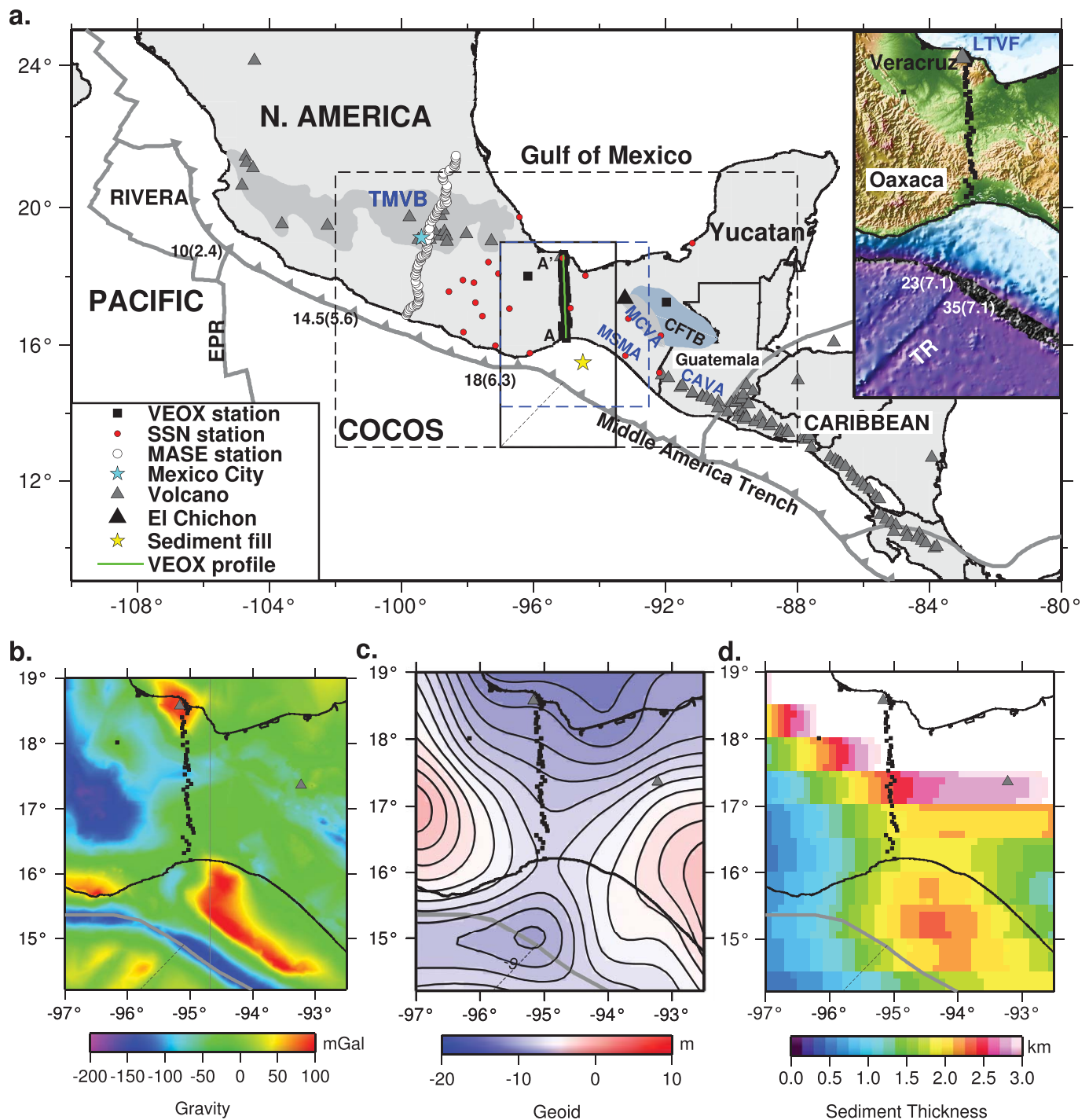


Figure 1. Map of southern Mexico. (a) Major tectonic feature of the study region. The age in Ma of the Cocos slab and the convergence rate in parentheses (in cm/yr) are shown along the Middle American Trench [Pardo and Suarez, 1995]. The yellow star indicates the location of reflection profile that determined the thickness of sediment fill [Ross and Shor, 1965]. The abbreviations shown in the map are TR, Tehuantepec ridge; LTVF, Los Tuxtlas Volcanic Field; EPR, East Pacific Rise; TMVB, Trans-Mexican Volcanic Belt; CFTB, Chiapas Fold and Thrust Belt; MCVA, Modern Chiapanecan Volcanic Arc; MSMA, Miocene Sierra Madre arc; CAVA, Central American Volcanic Arc. The upper-right inset shows the topographic and bathymetric map enclosing the station array (black box). Note the topographic low in the Tehuantepec Isthmus. (b) Free air offshore and Bouguer onshore gravity map of the study area (blue-dashed box in Figure 1a) [Manea and Manea, 2008]. (c) Geoid [Forste et al., 2008]. (d) Sediment thickness [Laske and Masters, 1997].

Earlier receiver function analyses [Melgar and Perez-Campos, 2010; Kim et al., 2011] suggest that the signature of the Cocos oceanic crust appears to be absent beyond ~150 km depth. Typically, the absence of seismic perturbations can be due to no effective velocity contrasts between anhydrous eclogite and mantle

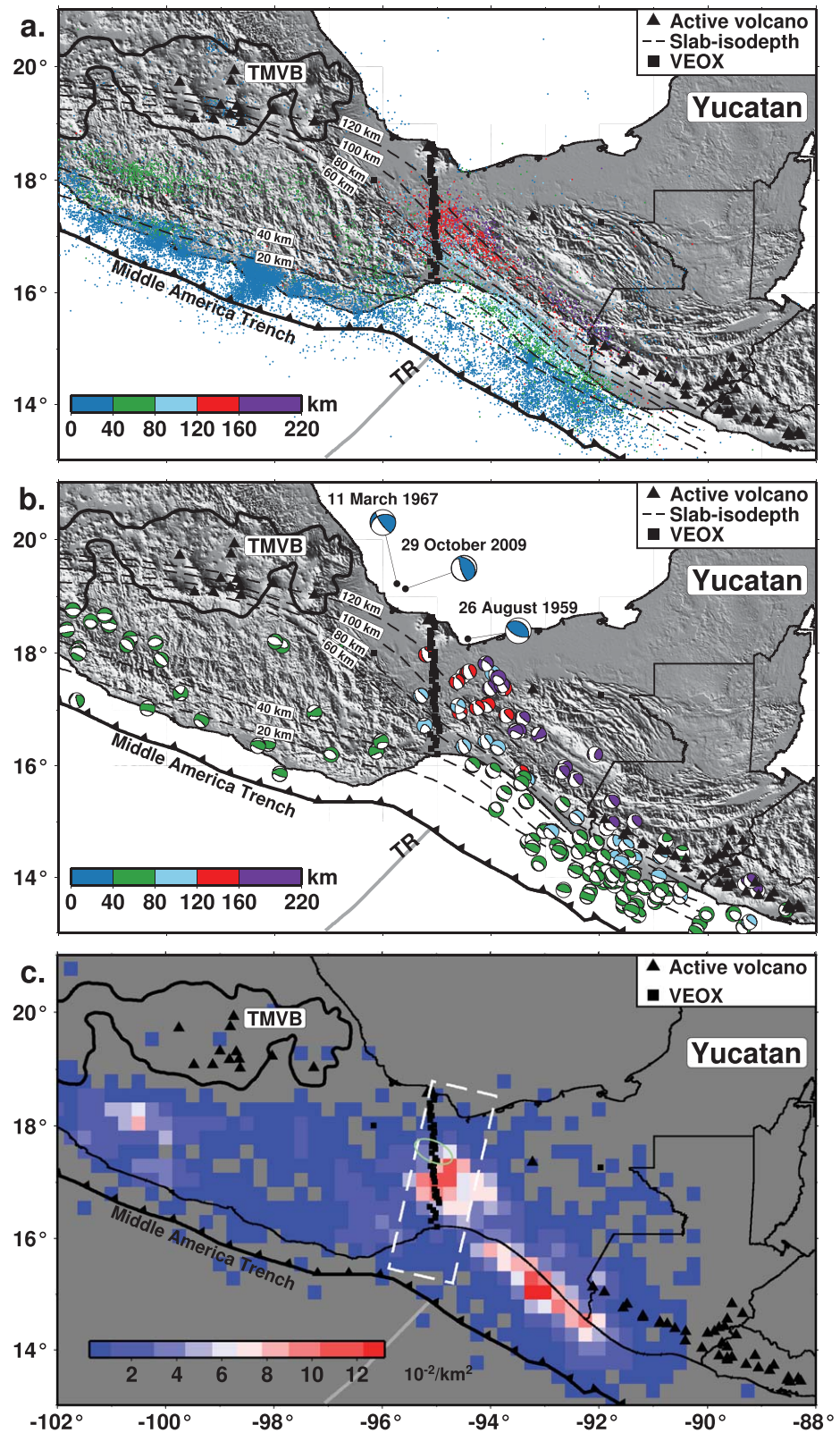


Figure 2.

peridotite [Bostock *et al.*, 2002, and references therein]. However, Kim *et al.* [2011] argued based on the receiver functions and modeling of their seismic observations that the Cocos slab has been truncated by the southwest-dipping slab. Furthermore, the Bayesian inversion of the receiver function amplitudes at the top and bottom of the oceanic crust suggests no trace of eclogite in the dipping crust of the Cocos plate beneath southern Mexico [Kim *et al.*, 2012a]. Recent tomographic images [Chen and Clayton, 2012] also support the image of the truncated Cocos slab.

In addition to significant along-strike slab-dip variations along the trench, a complex, discontinuous distribution of active volcanoes in the Mexican subduction zone clearly suggests complicated subduction dynamics. In central Mexico, a ~1000 km-long Neogene continental arc (Trans-Mexican Volcanic Belt, TMVB; Figure 1a) shows a large variation in composition and volcanic style [Ferrari *et al.*, 2012, and references therein]. The volcanic arc front is currently 40 km south of the Mexico City (Figure 1a) [Straub *et al.*, 2011], and previously published migration images show a steeply-dipping Cocos slab, at ~100 km depth beneath the arc front [Kim *et al.*, 2012b] in Central Mexico. On the other hand, in southern Mexico, the arc magmatism is absent from the expected arc location near the coast. Instead, the isolated Los Tuxtlas Volcanic Field (LTVF; Figure 1a, inset) is active to the north near the Gulf of Mexico, and the origin of volcanism in the LTVF is still unclear [e.g., Verma, 2006], although the composition of volcanic rocks are suggested to be calc-alkaline, similar to the TMVB [Ferrari *et al.*, 2012]. Also, the Modern Chiapanecan Volcanic Arc (MCVA; Figure 1a), which includes El Chichón, is oriented oblique to the trench axis and sits ~300 km from the trench.

1.2. Subduction of the Tehuantepec Ridge

A notable bathymetric feature offshore southern Mexico is the Tehuantepec ridge (TR), which is a relic fracture zone [Woodcock, 1975] (Figure 1) that appears as a bathymetric low with at least 2 km of sediment fill in the Gulf of Tehuantepec (Figure 1d, yellow star) [Ross and Shor, 1965]. A chain of high-amplitude gravity anomalies is located over the TR (Figure 1b) [Manea and Manea, 2008]. The TR separates the Cocos plate into two sections of different ages (Figure 1a, inset) [Klitgord and Mammerickx, 1982] and crustal thicknesses (12 km at NW of the TR and 9 km at SE of the TR; Woodcock [1975]).

Subduction of the TR is presumed to be the cause of the flat slab geometry [e.g., Gutscher *et al.*, 2000] found beneath Central Mexico [Perez-Campos *et al.*, 2008; Kim *et al.*, 2010, 2012b]. However, the subduction of the ridge does not appear to contribute to shallowing or flattening of the subduction dip angle of the Cocos slab in southern Mexico for the following two reasons. First, the flat slab subduction occurs along the MASE station profile, ~500 km west of the subducting ridge axis (Figure 1a) [Perez-Campos *et al.*, 2008; Kim *et al.*, 2010, 2012b, 2013]. Based on the seismicity (Figure 2a), the dip of the Cocos slab starts increasing beneath the region south of the northeastern end of the TMVB. The origin of this flat subduction beneath central Mexico is not apparent, but one possible cause is a change in the dynamics of subduction due to a change in mantle wedge viscosity from slab dehydration [e.g., Manea and Gurnis, 2007; Skinner and Clayton, 2010; Kim *et al.*, 2013]. Second, the geometry of the Wadati-Benioff zone beneath southern Mexico along the subducting ridge axis is defined as “normal” with the $>40^\circ$ dip [Rebollar *et al.*, 1999; Bravo *et al.*, 2004].

However, volcanism associated with El Chichón (age of 0.2 Myr) is suggested to be related to the subduction of the TR [Manea and Manea, 2008] although the slab is located 200–220 km beneath El Chichón [Bravo *et al.*, 2004], which might be too deep to be the source of the volcanism [Wada and Wang, 2009]. Geochemical characteristics in the volcanics from El Chichón suggest transitional calc-alkaline to adakitic magma [De Ignacio *et al.*, 2003], distinctively different from those in TMVB to the northwest and also trench-parallel Central American Volcanic Arc (CAVA; Figure 1a) to the southeast. Although the TMVB sits oblique to the trench (at $\sim 17^\circ$ to the strike

Figure 2. Topographic map showing regional seismicity in southern Mexico. The location of this map is shown in Figure 1a (black dashed box). (a) Seismicity based on the January 2006 to April 2014 SSN catalog. Depth of the earthquakes are color coded. Dashed contour lines represent the isodepth contours of the subducted Cocos slab in 20 km depth interval, constrained by local seismicity, and receiver functions [Perez-Campos *et al.*, 2008; Kim *et al.*, 2010]. Note the abrupt change from the Tehuantepec Isthmus, with seismicity decreasing and shallowing to the northwest. This directly corresponds to the location of the Cocos slab dip change from ~ 10 degrees to ~ 30 degrees (from W to E of the Tehuantepec Isthmus). (b) Selected focal mechanisms from global-CMT catalog [Dziewonski *et al.*, 1981; Ekström *et al.*, 2012], including three reverse faulting mechanisms near the southern margin of the Gulf of Mexico. (c) Density of earthquake events ($10^{-1}/\text{km}^2$) based on the seismicity shown in Figure 2a. The density of the seismicity is defined as the number per unit area of earthquakes on each bin (10×10 min over ~ 9 years of seismicity). We use the same earthquake data set used in Figure 2a but exclude the crustal seismicity (earthquakes shallower than 40 km). Note for high seismic activity focused at the middle of the VEOX array. The white-dashed box indicates the rough location of Tehuantepec Isthmus. Also, the location of the earthquake cluster at the depths 120–150 km is highlighted by a green ellipse.

of the trench), the top interface of the subducting Cocos slab at the start of the TMVB along the MASE line is at no more than ~ 100 km depth based on seismic images [Kim *et al.*, 2012b, 2013]. In addition, the intraslab earthquake distribution from Guatemala to the Yucatán Block does not show any significant change in slab dip (Figure 2a). All these independent pieces of evidence suggest that the change in the volcanism from the Modern Chiapanecan Volcanic Arc (MCVA; Figure 1a), which includes El Chichón, to the CAVA cannot be related to Cocos plate subduction alone, and thus must be associated with a separate tectonic process.

1.3. Motivation of the Study

The dense seismic array data set from the Veracruz-Oaxaca (VEOX) seismic line (Figure 1, black squares) is used to reveal several important constraints that may shed light on the unusual subduction dynamics in southern Mexico. First, an anomalous concentration of seismic activity in the Isthmus of Tehuantepec at intraslab event depths (Figure 2c) may be an indication of unusual slab dynamics. Second, previous seismic images show that the Cocos slab has been truncated at the depth of ~ 150 km by an anomalous southwest-dipping seismic anomaly dipping SW from the Gulf of Mexico [Kim *et al.*, 2011; Chen and Clayton, 2012]. Kim *et al.* [2011] hypothesize that this seismic anomaly was created by subduction of oceanic lithosphere prior to the collision of the Yucatán Block with Mexico at approximately 12 Ma. There is no established tectonic explanation for the south-dipping structure under the current paradigm of Caribbean plate reconstructions. Nevertheless, its presence and three-dimensional mantle flow beneath the subduction system (suggested from the Rayleigh wave analysis by Stubbailo *et al.* [2012]) may be able to clarify the cause of the overriding plate deformation in southern Mexico more evidently than from the standard model of the Cocos plate subduction.

In this paper, we provide a high-resolution image based on the migration of scattered teleseismic body waves [Bostock *et al.*, 2001, and references therein], along with new improved locations of local earthquakes [Waldhauser and Ellsworth, 2000] to better constrain the seismic velocity structures at uppermost mantle depths (< 200 km) beneath southern Mexico. This migration technique provides the clearest available images of the Cocos slab, and provides insight into the process of subducting relatively young Cocos oceanic lithosphere. Although the imaged feature is not as sharp as the Cocos plate, the same images show the southwest dipping structure from the Gulf of Mexico, which supports previous seismic observations and interpretations [Kim *et al.*, 2011; Chen and Clayton, 2012] and may explain overriding-plate deformation in response to interaction with this structure. Also, the images will clarify the relationship between seismicity and the newly observed seismic anomalies.

2. Data Analysis and Methods

In order to accurately define the subduction zone structure, we use the two-dimensional generalized radon transform-based migration (hereafter 2-D GRT) method and relocate local seismicity. First, we use the 2-D GRT method to identify the location and magnitude of the discontinuities separating regions of differing seismic impedance. This method inverts scattered waves within the teleseismic P-wave coda for sharp variations in the Earth's elastic properties beneath high-density arrays [Bostock and Rondenay, 1999; Bostock *et al.*, 2001; Rondenay *et al.*, 2005; Rondenay, 2009]. The method has been extensively applied to array data sets in various subduction zones to constrain seismic properties in the subduction system and also to infer subduction dynamics (e.g., Alaska [Rondenay *et al.*, 2008, 2010; Kim *et al.*, 2014], Cascadia [Bostock *et al.*, 2002; Abers *et al.*, 2009], Costa Rica and Nicaragua [MacKenzie *et al.*, 2010], western Hellenic [Suckale *et al.*, 2009; Pearce *et al.*, 2012], and central Mexico [Kim *et al.*, 2012b, 2013]). This method has been previously applied to the central Mexico data set [MASE, 2007], where Kim *et al.* [2012b] described the imaging procedure in detail.

Second, we improve the precision of earthquake location by using the double difference hypocenter algorithm (hypoDD) [Waldhauser and Ellsworth, 2000]. The double-difference algorithm uses relative travel times between event pairs and iteratively adjusts the locations of the events to minimize the sum of travel-time residuals. This approach thus allows large areas of seismicity to be relocated simultaneously. The algorithm determines the relative hypocenters so that they can be less affected by uncertainty in phase picking and velocity structure. The resulting relative hypocentral errors are ~ 0.1 km in epicenter and ~ 0.25 km in depth [Ellsworth *et al.*, 2000]. The local seismicity is relocated using the same one-dimensional background velocity model (Table 1) [Kennett and Engdahl, 1991] as the one used in the 2-D GRT imaging to minimize the differences in depth between the earthquakes and the imaged structures.

Table 1. One-Dimensional Reference Model for Migration [Kennett and Engdahl, 1991]

Layer	Depth Ranges (km)	V_p (km/s)	V_s (km/s)	Density (g/cm ³)
1	0–20	5.8	3.36	2.85
2	20–40	6.5	3.75	2.90
3	40–190	8.04	4.47	3.34

2.1. Teleseismic Imaging

We follow stringent data selection and pre-processing steps for the migration, described in Pearce et al. [2012] and Kim et al. [2012b], and retrieve 15 high-quality teleseismic P waves recorded from 45 seismometers in the VEOX seismic line with an average interstation distance of about 6–8 km (Figure 3a). The migration requires

an incident P wave arrival that can be identified across the majority of the stations [e.g., Pearce et al., 2012]. Among these 15 earthquakes, we select only five earthquakes in quadrant 2 (E and SE of the VEOX line; Figure 3d) to examine the southwest-dipping seismic anomaly, whereas 20 earthquakes are previously used to image the anomaly with receiver functions [Kim et al., 2011].

In the migration images, inversions determine the velocity perturbations with respect to the background velocity field (Table 1) [Kennett and Engdahl, 1991] needed to produce the scattered wavefield [Rondenay et al., 2001, 2005]. The 2-D GRT simultaneously inverts a combination of scattering (forward and backscattered) modes using analytical expressions for their traveltimes and amplitudes [Bostock et al., 2001]. The scattering modes are defined as the incident P wave forward scattered as an S wave (Ps); the free-surface-reflected P wave backscattered as an S wave (PpPs); and the free-surface-reflected S wave backscattered as an Sv wave (PpSs|v) and Sh wave (PpSs|h). The four scattering modes are sensitive to S wave velocity perturbations and are combined to form a single composite image. S-wave velocity perturbations are shown with a red to blue color scale, which represents negative (slower) to positive (faster) velocity perturbations (Figures 3b, 3c, 3e, and 3f). Velocity discontinuities in the migration images are identified by crossovers in the color scale, with red-to-blue denoting an increase in velocity with depth (e.g. Moho) and blue-to-red denoting a decrease in velocity with depth [Rondenay et al., 2005].

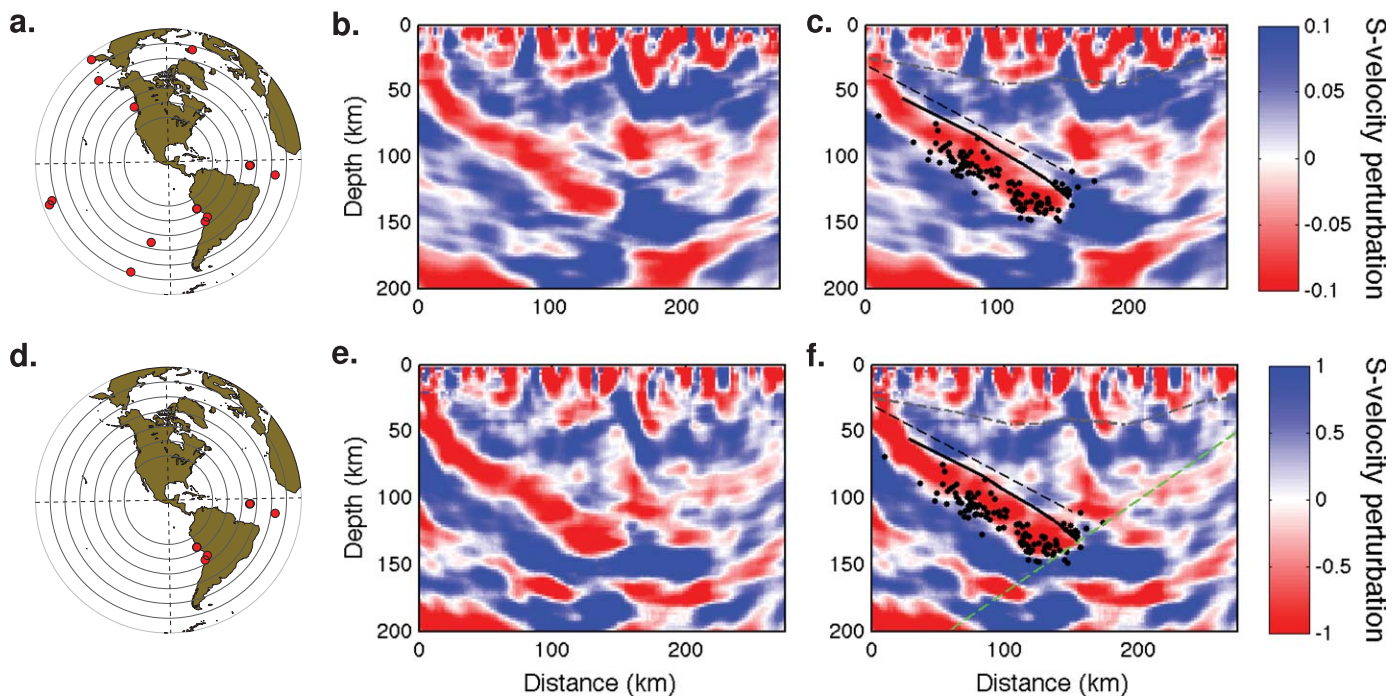


Figure 3. Azimuthal contributions to the S-velocity perturbation (dV_s/V_s) images. Quadrants are defined relative to the azimuth of station transect. (a) Event map showing all teleseismic earthquake locations. (b) The dV_s/V_s image based on the events shown in Figure 3a. (c) The image (same as Figure 3b) with relocated seismicity (shown as black dots) and interpretation lines. The black solid line represents the top interface of the Cocos plate based on the image, and the dashed line from previous receiver function results [Kim et al., 2011]. (d) Event map showing teleseismic earthquakes located in quadrant 2. (e) The dV_s/V_s image based on the events shown in Figure 3d. (f) The image (same as Figure 3e) with relocated seismicity and interpretation lines. The green-dashed line represents the location of the positive receiver function amplitudes [Kim et al., 2011].

The signal-to-noise ratio (SNR) is generally lower for most of the stations compared to the SNR from *MASE* [2007] in *Kim et al.* [2012b], which is why only 15 earthquakes were used to produce these migration images. In particular, the data quality is poor for stations near the Pacific coast due to frequent flooding events during the data collection period (2007–2008; *Kim et al.* [2011]). Thus, *Melgar and Perez-Campos* [2010] and *Kim et al.* [2011] apply a frequency band from 0.08 to 0.33 Hz to reduce such noise near the coastal stations to constrain the geometry of the Cocos slab. For migration, we use a similar filter range (0.03–0.3 Hz) to effectively sample backscattered phases and to enhance image coherence.

The migrated scattered-wave image roughly shows the presence of opposing structures with different magnitudes although each response is rarely clear. On its own, the Ps modes recover the dipping structures the best because the Ps mode is most sensitive to steeply dipping features; however, it does not resolve the thickness of the dipping layer (7–10 km based on previous receiver function results [*Melgar and Perez-Campos*, 2010; *Kim et al.*, 2011]) due to the lower frequency filter of 0.03–0.3 Hz used in the migration and the lower volume resolution of the Ps mode [*Rondenay et al.*, 2005]. We apply different weights to the four scattering modes (5 for Ps, 2 for PpPs, 0.5 for PpSs|v, and 0.5 for PpSs|h) to reduce the contributions from scattering modes that display weak responses [*Rondenay et al.*, 2001].

For imaging, we set a profile azimuth of -2° along the VEOX station transect (A-A' in Figure 1a). Various projection angles are tested to recover the oppositely-dipping structure, and we find that the azimuth of -2° , closest to the station array line, returns the most focused signal. As the projection angle deviates from the angle for A-A', migration artifacts such as "migration smiles" appear due to insufficient spatial sampling. This might be due to the very small number of earthquakes used in the migration that originate from only one side from the VEOX array.

We divide the events in four backazimuth groups to examine azimuthal contribution to the migration image. Since the proposed structure [*Kim et al.*, 2011; *Chen and Clayton*, 2012] is southwest-dipping, the events from quadrant 2 (Figure 3d) are necessary to image such an anomaly [*Kim et al.*, 2011]. *Kim et al.* [2011] demonstrate that the image of the southwest dipping structure is degraded if all the backazimuth data (e.g., Figure 3a) are included in the image. We also observe that the event contributions from quadrant 2 (mostly from E and SE of the VEOX array) are essential to image the southwest-dipping structure. For this reason, we show two images: one with all contributions (Figures 3b and 3c) and the other with only the events from E and SE (Figures 3e and 3f).

2.2. Seismicity Relocation

The relocation of local seismicity illuminates the extent of structures into the upper mantle and thus better defines the Wadati-Benioff zone geometry. We relocate regional earthquakes recorded from the VEOX (operated from September 2007 to March 2009) and permanent Servicio Sismológico Nacional (SSN) networks, which broadly cover the study region (Figure 1a, red circles). We include the data from the SSN to further enhance the spatial (lateral) resolution and to accurately define the cross-dip of the Cocos slab. We select event pairs with a hypocentral separation of less than 30 km and hypocentral distances of less than 300 km. We employ the least-squares conjugate gradient method (LSQR) for relocating large data sets as defined in *Waldhauser and Ellsworth* [2000] and waveform cross correlation to obtain the differential arrival times.

A total of 1129 earthquakes from the SSN network and 164 from the SSN and VEOX were relocated using hypoDD [*Waldhauser and Ellsworth*, 2000]. We examine this relocated data set in map view and with 11 cross sections parallel to the slab dip direction (Figure 4a) and eight profiles along the station transect (Figure 4a; parallel to a profile A-A' in Figure 1a). The earthquakes plotted in Figure 4b are selected from epicenters within 10 km of each profile. The relocated events provide a clear image of the Cocos plate Benioff zone down to depths greater than 100 km (Figure 4b, all profiles) and an anomalous concentration of seismic activity at depths between 100 and 150 km (Figure 4b, profiles 3, 4, and 13–16). Note that the seismicity following the trend of the oppositely-dipping structure is better seen from the projection profiles parallel to A-A' shown in Figure 1a (Figure 4b).

3. Imaged Seismic Anomalies

Previous estimates of the depth extent and dip of the Cocos slab slightly disagree depending on the methods used. Sharp subduction interfaces (assuming substantial velocity contrast across the interfaces) can be

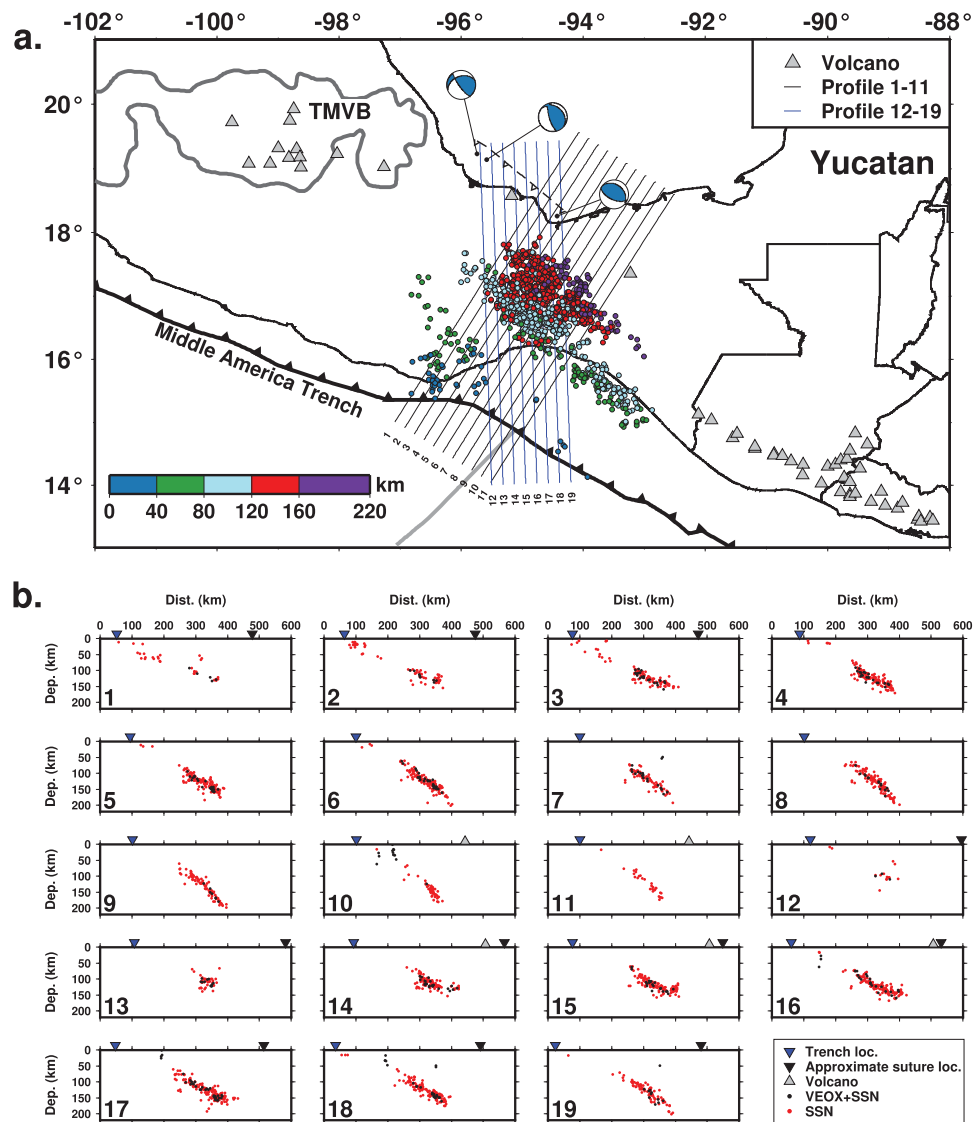


Figure 4. Relocated seismicity. (a) Profile locations and relocated seismicity, color-coded by depth in a map view. A rough surface suture zone [Kim *et al.*, 2011] and three high-angle reverse faulting mechanisms [Franco *et al.*, 2013] are plotted at the southern margin of the Gulf of Mexico. The profiles are chosen perpendicular to the trench (profiles 1–11) and parallel to the VEOX station array (profiles 12–19) to examine the subducting Cocos plate and the seismic concentration at the depth of 150 km. (b) Relocated seismicity along different profiles.

resolved by using the converted seismic phases. The receiver function studies based on the Ps phase by Melgar and Perez-Campos [2010] and Kim *et al.* [2011] trace a single negative conversion at the top of the Cocos oceanic crust down to ~150 km. Both studies filter the seismic data down to 0.3 Hz to enhance this feature. Utilization of essentially the same data set, but by examination of backazimuthal contributions in the image, Kim *et al.* [2011] argue that the Cocos slab was detached by the oppositely-dipping structure. This seismic structure was suggested to be a slab based on clear positive receiver function amplitudes, dipping at 35 degrees SSW from Gulf of Mexico [Kim *et al.*, 2011]. Such positive conversions appear to be sharp at higher frequencies (~1.0 Hz); however, the termination depth of the positive conversion trend is ambiguous due to poor data quality near the Pacific coast [Kim *et al.*, 2011]. A P-wave velocity reduction of ~20% with respect to the oceanic mantle velocity is required to reproduce such strong conversions [Kim *et al.*, 2011]. Tomographic images by Chen and Clayton [2012] also show a sharp image of this enigmatic structure dipping from the Gulf of Mexico, shown as a fast velocity anomaly (<5% P-wave velocity perturbation with respect to the 1-D velocity model) beneath the VEOX array in addition to the image of the Cocos slab with a

similar velocity perturbation estimate. Their synthetic recovery test demonstrates that the velocity anomalies dipping from either side can be well-resolved with only slight smearing [Chen and Clayton, 2012]. The opposite-dipping structure is imaged to have a 10° steeper dip than the receiver function based estimate by Kim *et al.* [2011] (see Chen and Clayton [2012] Appendix for discussion on the dip discrepancy between different methods), and its termination depth is not as well-constrained due to the depth limitation of their data set.

3.1. Migration Images

Because of the significant azimuthal dependency in the image of the oppositely-dipping structure [Kim *et al.*, 2011], we use the events in the east and southeast from the VEOX array (Figure 3d) to constrain its geometry. Although the image of the oppositely-dipping structure appears less sharp than that of the Cocos slab (Figures 3e and 3f), this image still shows the two opposing structures. The migration provides higher accuracy than the receiver function method based on upgoing Ps seismic mode only [Langston, 1979, and references therein] in terms of the subsurface location, volume, and dip of the low-velocity anomaly because it is a prestack method based on the scattering theory, and so is capable of imaging steeply ($< \sim 60^\circ$) dipping structures [Bostock *et al.*, 2001; Rondenay *et al.*, 2005]. The same image also contains the dipping Cocos slab, and the slab is moderately well-imaged as a low velocity layer regardless of different event contributions to the migration (Figures 3b and 3e).

The magnitudes of the converted phases from the interface in the oppositely-dipping structure are much weaker and somewhat discontinuous than those produced by the Cocos slab. Such weak conversions (negative amplitudes) along the interface might be due to the small impedance contrast across the interface as noted by Kim *et al.* [2011], and/or small number of earthquakes for imaging the seismic structures. Since only five teleseismic events were used in one azimuth bin (Figure 3d), these may not be sufficient to sharply constrain its geometry nor constrain the depth extent. In addition, the smaller lateral dimension of this dipping structure (in comparison to the Cocos slab) may also contribute to the weaker converted signals at the top interface. The green-dashed line in Figure 3f delineates positive amplitudes of the receiver functions (7–8 km below the interface with weak negative conversions; Kim *et al.* [2011]).

The lower frequency band used in the migration is more effective for constraining the geometry of the Cocos slab, as has also been observed in receiver function images [Kim *et al.*, 2011]. Our image shows the subducting Cocos slab (Figure 3c, black solid line) dipping at $\sim 30^\circ$, which is $4\text{--}5^\circ$ steeper than previous estimates from receiver functions (Figure 3c, black-dashed line). The structural location and dip of the imaged low-velocity Cocos oceanic crust do not change considerably with different event contributions to the migration. When a high weight on the Ps mode is used with the lower frequency content in the preprocessed data, the thickness of the low-velocity anomalies is estimated to be ~ 20 km, much thicker than offshore refraction data (7–8 km by Shor and Fisher [1961]) and previous receiver function results (7–10 km by Melgar and Perez-Campos [2010] and Kim *et al.* [2011]). Additionally, it can be argued that the thickness cannot be resolved due to the lower volume resolution of Ps mode [Rondenay *et al.*, 2005].

It is also important to note that the major difference from the previous receiver function results is that the oceanic crust sits 11 km deeper than the previous estimate [Melgar and Perez-Campos, 2010; Kim *et al.*, 2011]. This depth discrepancy may be due to the different background models used in the different methods.

3.2. Relocated Seismicity

The distribution of seismicity has previously provided the most robust way to characterize the geometry of the subducted Cocos plate beneath the Isthmus of Tehuantepec [Pardo and Suarez, 1995; Rebolgar *et al.*, 1999; Bravo *et al.*, 2004]. We show our seismicity relocations along profiles parallel and oblique to the station array (Figure 4a) to examine (1) the geometry of the dipping structures in addition to the constraints from the converted seismic phases discussed in section 3.1, (2) the cross-dip of the Cocos slab, and (3) the coupled zone of the Cocos slab and the overriding North American plate from west to east. Figure 4a shows the location of the two series of profiles, which are trench-perpendicular or parallel to the down-dip axis of the TR and the Cocos slab (profiles 1–11) and parallel (profiles 12–19) to the station array.

The profiles perpendicular to the trench show a significant change in along-strike direction of the Cocos slab in the down-dip direction (Figure 4b). Profiles 1–11 show a change of more than 15° in slab dip, which is also shown with slab surface contour lines based on seismicity and receiver functions (Figure 2a and 2b). The dip

of the Cocos slab beneath southern Mexico (from the profile 7) is estimated to be $\sim 30^\circ$, consistent with the results by *Pardo and Suarez* [1995]. The dip of the slab continues to increase to the east (Figure 4b). These profiles show a more rapidly decreasing trend in the cross dip of the Cocos slab in the NW-SE directions.

The distribution of seismicity in profiles 13–16 (between $17.4\text{--}17.7^\circ\text{N}$ and $94.5\text{--}95.5^\circ\text{W}$ as shown in Figure 4a) define the subducting Cocos slab, and clearly show that the earthquakes terminate around 150 km and then extend to shallower depths (~ 30 km shallower), following the dipping trend of the structure that *Kim et al.* [2011] imaged (Figure 3f, green-dashed line). A concentration or cluster of seismic activity at depths greater than 80 km (Figure 2c) broadly cover this region. The relocated seismicity also correlates well with dipping low-velocity features at depths down to 150 km, shown in seismic images at the projection angle of -2° (Figures 3c and 3f).

The origin of the cluster of intermediate-depth earthquakes is not entirely clear, but the correlation with the location of depth change (upwards extent) of intermediate-depth seismicity may indicate a change in the slab geometry, that could produce the stress concentration necessary for this cluster. This anomalous seismic activity beneath southern Mexico does not correlate with the position of the active arc (Figure 2c; ~ 220 km away from the TMBV and MCVA), so a dehydration source can be ruled out.

3.3. Focal Mechanisms

3.3.1. Subducted Cocos Slab-Related Earthquakes

Selected focal mechanisms from the global-CMT catalog [*Dziewonski et al.*, 1981; *Ekström et al.*, 2012] since 1976 (with depths greater than 40 km) are plotted and shown in Figure 2b. As discussed in *Rebollar et al.* [1999], the focal mechanisms calculated from shallow earthquakes in southern Mexico are indicative of normal faulting at the outer rise of the Cocos plate and compression at the trench. The earthquakes located at the contact of subducting and overriding plates generally show thrust faulting (Figure 2b). In contrast, the focal mechanisms from the intermediate-depth (50–160 km) earthquakes indicate that the subducted Cocos slab is under extensional stress (Figure 2b). Yet at depths greater than 200 km in the southeast of the VEOX stations, the subducted lithosphere is under compression [*Rebollar et al.*, 1999].

3.3.2. High-Angle Reverse Faulting Events at the Southern Margin of Gulf of Mexico

Although sparse, several shallow earthquakes are identified near the southern margin of the Gulf of Mexico (Figures 2a and 2b) [*Franco et al.*, 2013]. The mechanisms indicate reverse faulting at high angles (dip of $\sim 45^\circ$) with the axes of maximum compression oriented northwest to southeast at depths less than 30 km [*Suarez*, 2000; *Suarez and Lopez*, 2011]. Since the Gulf is located far from the active Pacific margin, the deeper depth events (depth less than 70 km) are previously considered to be intraslab earthquakes [*Franco et al.*, 2013]. *Suarez* [2000] and *Suarez and Lopez* [2011] also suggest that the shallow events (depth less than 70 km) are due to the subduction of the Tehuantepec ridge on the Cocos slab enhancing stress accumulation. However, these earthquakes occur at the mantle or lower crustal depths (assuming the crust is 20 km thick [*Buffler*, 1991]), and thus this may be due to the tectonic movement associated with the Yucatán Block.

4. Discussion

The dip of the imaged anomaly with opposite polarity is $\sim 30\text{--}35^\circ$ based on migration and seismicity (Figure 3), and its termination depth is not sharply determined, whereas previous receiver functions determine its dip of 35° , a total length of ~ 250 km along the VEOX transect [*Kim et al.*, 2011]. Regardless of the limited resolution due to insufficient data sampling, our migration images support the results of *Kim et al.* [2011], discussed in section 3.1. The origin of this anomalous structure is still unclear. In sections 4.1 and 4.2, we highlight several issues that are not discussed in the previous papers.

4.1. Imaged Seismic Anomaly and Its Relationship to the Overriding Plate Structure

Our image of the opposing structures (Figure 3e) (Figure 9b of *Kim et al.* [2011]; Figures 7 and 12 of *Chen and Clayton* [2012]) clearly shows room for asthenospheric mantle to intrude beneath the subduction system. Furthermore, these images show that the southwest-dipping anomaly is at ~ 100 km depth directly beneath the El Chichón volcanic center. Thus, this suggests that the volcanism of the El Chichón might be more related to this anomaly although the structure of the slab-mantle interface and its seismic properties need to be better constrained by processing seismic signals recorded in the Yucatán Block to confirm this inference. Coupled with the flat slab process ~ 25 Ma in central Mexico [*Ferrari et al.*, 2012, and references

therein], the arc-parallel mantle wedge flow in NW-SE direction beneath the Yucatán Block should be significant enough to form nontrench parallel MCVA in addition to the slab melting to generate the adakitic magma in El Chichón. To fully understand the 3-D system of this complex subduction zone, we would need in addition shear wave splitting results to enlighten the 3-D mantle flow beneath southern Mexico, which is beyond the scope of this study.

Previously the convergence of the Tehuantepec ridge (TR) is used to explain a complex pattern of deformation in the overriding North American plate because of its nearly perfect alignment with the El Chichón volcanic center in MCVA [Bravo *et al.*, 2004, and references therein]. Also, its convergence is suggested to result in the formation of the CFTB [Keppie and Moran-Zenteno, 2005; Mandujano-Velazquez and Keppie, 2009]. Nevertheless, the topographic low and discontinuous arc configuration in the Tehuantepec Isthmus (Figure 1), unusual geochemical signatures in El Chichón magmatism, and the shortening of more than 100 km over a very short-time interval (C. 2.5 Ma) by the formation the CFTB [Mandujano-Velazquez and Keppie, 2009] are difficult to explain by the subduction of the TR asperity on the Cocos plate.

First, there is a nonspatial symmetry in both tectonic and volcanic features with respect to the ridge axis of the TR. The topographic-low feature only exists to the west of the TR (Figure 1, inset). Also, current (nontrench-parallel) discontinuous arc locations (Figure 1) and the presence of an older extinct arc along the coast beyond the topographic-low region may be suggestive of more complicated slab dynamics. Furthermore, the presence of CFTB and its very short formation timing presents a problem for understanding the tectonic model in the area. The CFTB is only confined to the east of the projected ridge axis with its restricted size (300 × 600 km; see bluish gray region in Figure 1a). Such restricted spatial dimensions and short formation period of the CFTB may indicate that it is not caused by the subduction of the TR.

Second, volcanism in MCVA, LTVF, and at El Chichón do not appear to be the result of normal Cocos slab dehydration because the Cocos slab extends at least to 200 km below all of these volcanic centers (assuming that the Cocos slab is not detached). Our images along with the previously published seismic images suggest that the Cocos plate may be missing beneath these volcanic centers. In particular, the magma from the very young El Chichón volcano is both mineralogically and geochemically distinct from the volcanoes of TMVB and CAVA [De Ignacio *et al.*, 2003]. The magma contains magmatic anhydrite, and high water content (4–10 wt%) and oxygen fugacities, which are absent in the normal-arc rocks of the TMVB and CAVA [De Ignacio *et al.*, 2003]. A significant amount of water in the magma is difficult to explain by typical dehydration of the subducted sediment and basaltic oceanic crust alone. In fact, such features are common in adakites, and require partial melting of a subducting plate under high water fugacity conditions and partial melting of the mantle wedge [De Ignacio *et al.*, 2003].

Several authors have previously proposed the following in order to explain the magmatism of El Chichón at the unexpected location, far inland from the trench (Figure 1a): (1) extensional tectonics associated with the triple junction between the North America, Caribbean, and Cocos plates [Nixon, 1982], (2) a major change in plate configuration (such as a slab tear) [De Ignacio *et al.*, 2003], (3) strike-slip tectonic motion across the arc [García-Palomo *et al.*, 2004], and (4) strong serpentinization of the TR [Manea and Manea, 2008]. De Ignacio *et al.* [2003] suggest that a source of hot asthenospheric mantle from the slab tear allows the eastward intake of asthenosphere beneath the Yucatán Block, which induces melting of the subducting plate. However, the cessation of the along-arc volcanism in Miocene Sierra Madre Arc (MSMA) at 9–3 Ma [Damon and Montesinos, 1978] cannot be supported by any of the models listed above.

4.2. Origin of Intermediate-Depth Seismicity

In southern Mexico, a concentration of seismicity over a < 50 km wide window (17.4–17.7°N and 94.5–95.5°W; Figures 2c and 4a) follows the trend of the south-west dipping structure starting at the intersection point with the north-east dipping Cocos slab (Figures 3c and 3f; Figure 4b, profiles 13–16). This clustering occurs within a limited zone, and thus can only be seen with dense coverage of seismic stations. We suggest that the earthquake clustering may be due to the subduction of the TR [e.g., Pennington, 1981], and/or due to the presence of the imaged seismic anomaly [Kim *et al.*, 2011].

Previously, Manea and Manea [2008] suggested strong serpentinization of the TR to explain the unusual volcanism of El Chichón in terms of its geochemistry and presence of Cocos slab at >200 km depth (exceeding common depth of slab-mantle decoupling for the arc magmatism, as suggested by Wada and Wang

[2009]). This requires significant addition of fluids along faults at the outerrise of the TR, similar to the situation in Costa Rica [e.g., Ranero *et al.*, 2003]. If this is the case, the slab may be significantly weakened by active fluid migration to induce such seismic clustering.

There are very few earthquakes at mantle depths near the southern margin of the Gulf, and also high-angle reverse mechanism earthquakes in the approximate location of the suture zone [Kim *et al.*, 2011] or the surface projection of the southwest-dipping structure along the offshore margin close to the Gulf of Mexico (Figures 2b and 4a) [Franco *et al.*, 2013]. This may suggest that the high concentration of seismicity at intermediate focal depths is related to the anomalous seismic structure. However, in order to confirm this point, extensive seismic surveys near the southern margin of the Gulf and Yucatán Block are necessary.

5. Conclusions

The presence of the southwest-dipping structure provides new understanding on unusual tectonic and volcanic features in southern Mexico, although its origin is not apparent. The primary evidence comes from teleseismic migration of scattered P-wave coda and relocated regional seismicity together with previously published receiver function and travel-time tomography images along a 275 km seismic line from the Pacific coast to the Gulf of Mexico across the Isthmus of Tehuantepec. We provide the most focused image of the Cocos slab, which subducts at 30° with its leading edge present at 150 km depth. Although not as clearly imaged as the Cocos slab, we also trace a southwest-dipping structure, which dips in the opposite sense from the Gulf of Mexico, and currently has no known role in Caribbean tectonics. The relocated seismicity follows the trend of the Cocos slab and also this enigmatic structure starting at the intersection point with the Cocos slab at the depth of 150 km.

Acknowledgments

Y.K. and H.L. were funded by the Korea Meteorological Administration Research and Development Program under Grant CATER-2013-8010. M.S.M. was funded by NSF EAR-1054638. Authors thank entire VEOX team for making the data available. Finally, authors thank the editor and anonymous reviewers for helpful comments, which greatly improved the paper.

References

- Abers, G. A., L. S. MacKenzie, S. Rondenay, Z. Zhang, A. G. Wech, and K. C. Creager (2009), Imaging the source region of Cascadia tremor and intermediate-depth earthquakes, *Geology*, *37*(12), 1119–1122, doi:10.1130/G30143A.1.
- Bostock, M. G., and S. Rondenay (1999), Migration of scattered teleseismic body waves, *Geophys. J. Int.*, *137*, 732–746, doi:10.1046/j.1365-246x.1999.00813.x.
- Bostock, M. G., S. Rondenay, and J. Sharagge (2001), Multiparameter two-dimensional inversion of scattered teleseismic body waves: 1. Theory for oblique incidence, *J. Geophys. Res.*, *106*(B12), 30,771–30,782, doi:10.1029/2001JB000330.
- Bostock, M.G., R. D. Hyndman, S. Rondenay, and S. M. Peacock (2002), An inverted continental Moho and the serpentinization of the forearc mantle, *Nature*, *417*, 536–538.
- Bravo, H., C. J. Rebolgar, A. Uribe, and O. Jimenez (2004), Geometry and state of stress of the Wadati-Benioff zone in the Gulf of Tehuantepec, Mexico, *J. Geophys. Res.*, *109*, B04307, doi:10.1029/2003JB002854.
- Buffler, R. T. (1991), Seismic stratigraphy of the deep Gulf of Mexico basin and adjacent margins, In *The Gulf of Mexico Basin. The Geology of North America*, edited by A. Salvador, pp. 353–387, Geol. Soc. of Am., Boulder, Colo.
- Chen, T., and R. W. Clayton (2012), Structure of central and southern Mexico from velocity and attenuation tomography, *J. Geophys. Res.*, *117*, B09302, doi:10.1029/2012JB009233.
- Damon, P. and E. Montesinos (1978), Late Cenozoic volcanism and metallogenesis over an active Benioff Zone in Chiapas, Mexico. *Ariz. Geol. Soc. Dig.*, *11*, 155–168.
- De Ignacio, C., P. Castineiras, A. Marquez, R. Oyarzun, J. Lillo, and I. Lopez (2003), The El Chichón volcano (Chiapas volcanic belt; Mexico), transitional calc-alkaline to adakitic-like magmatism: petrologic and tectonic implications, *Int. Geol. Rev.*, *45*, 1020–1028, doi:10.2747/0020-6814.45.11.1020.
- DeMets, C., and S. Stein (1990), Present-day kinematics of the Rivera plate and implications for tectonics in southwestern Mexico, *J. Geophys. Res.*, *95*(B13), 21,931–21,948, doi:10.1029/JB095iB13p21931.
- Dziewonski, A. M., T.-A. Chou and J. H. Woodhouse (1981), Determination of earthquake source parameters from waveform data for studies of global and regional seismicity, *J. Geophys. Res.*, *86*(B4), 2825–2852, doi:10.1029/JB086iB04p2825.
- Ekstrom, G., M. Nettles, and A. M. Dziewonski (2012), The global CMT project 2004–2010: Centroid-moment tensors for 13,017 earthquakes, *Phys. Earth Planet Inter.*, *200–201*, 1–9, doi:10.1016/j.pepi.2012.04.002.
- Ellsworth, W. L., B. R. Julian, F. Klein, A. J. Michael, D. H. Oppenheimer, S. G. Prejean, K. Richards-Dinger, S. L. Ross, D. P. Schaff, and F. Waldhauser, (2000), Seismicity of the San Andreas Fault system in central California: Application of the double-difference location algorithm on a regional scale, *Eos Trans. AGU*, *81*(48), Fall Meet. Suppl., Abstract S21D-01.
- Ferrari, L., T. Orozco-Esquivel, V. Manea, and M. Manea (2012), The dynamic history of the Trans-Mexican Volcanic Belt and the Mexico subduction zone, *Tectonophysics*, *522–523*, 122–149, doi:10.1016/j.tecto.2011.09.018.
- Forste, C., et al. (2008), The GeoForschungsZentrum Postdam/Groupe de Recherche de Geodesie Spatiale satellite-only and combined gravity field models: EIGEN-GL04S1 and EIGEN-GL04C. *J. Geod.*, *82*, doi:10.1007/s00190-007-0183-8.
- Franco, S. I., C. Canet, A. Iglesias, and C. Valdes-Gonzalez (2013), Seismic activity in the Gulf of Mexico. A preliminary analysis, *Bol. Soc. Geol. Mex.*, *65*(3), 447–455.
- García-Palomos, A., J. L. Macías, and J. M. Espíndola (2004), Strike-slip faults and K-Alkaline volcanism at El Chichón volcano, southeastern Mexico, *J. Volcanol. Geotherm. Res.*, *136*, 247–268.
- Gutscher, M. A., W. Spakman, H. Buwaard, and E. R. Engdahl (2000), Geodynamics of flat subduction: Seismicity and tomographic constraints from the Andean margin, *Tectonics*, *19*(5), 814–833, doi:10.1029/1999TC001152.

- Keppie, J. D., and D. J. Moran-Zenteno (2005), Tectonic implications of alternative Cenozoic reconstructions for Southern Mexico and the Chortis Block, *Int. Geol. Rev.*, *47*, 473–491.
- Kennett, B. L. N., and E. R. Engdahl (1991), Traveltimes for global earthquake location and phase identification, *Geophys. J. Int.*, *105*(2), 429–465.
- Kim, Y., R. W. Clayton, and J. M. Jackson (2010), The geometry and seismic properties of the subducting Cocos plate in central Mexico, *J. Geophys. Res.*, *115*, B06310, doi:10.1029/2009JB006942.
- Kim, Y., R. W. Clayton, and F. Keppie (2011), Evidence of a collision between the Yucatán Block and Mexico in the Miocene, *Geophys. J. Int.*, *187*, 989–1000, doi:10.1111/j.1365246X.2011.05191.x.
- Kim, Y., R. W. Clayton, and J. M. Jackson (2012a), Distribution of hydrous minerals in the subduction system beneath Mexico, *Earth Planet. Sci. Lett.*, *341–344*, 58–67, doi:10.1016/j.epsl.2012.06.001.
- Kim, Y., M. S. Miller, F. D. Pearce, and R. W. Clayton (2012b), Seismic imaging of the Cocos plate subduction zone system in central Mexico, *Gechem. Geophys. Geosyst.*, *13*, Q07001, doi:10.1029/2012GC004033.
- Kim, Y., R. W. Clayton, P. D. Asimow, and J. M. Jackson (2013), Generation of talc in the mantle wedge and its role in subduction dynamics in central Mexico, *Earth Planet. Sci. Lett.*, *384*, 81–87, doi:10.1016/j.epsl.2013.10.006.
- Kim, Y., G. A. Abers, J. Li, D. Christensen, J. Calkins, and S. Rondenay (2014), Alaska Megathrust 2: Imaging the megathrust zone and Yakutat/Pacific plate interface in the Alaska subduction zone, *J. Geophys. Res.*, *119*, 1924–1941, doi:10.1002/2013JB010581.
- Klitgord, K. D., and J. Mammerickx (1982), Northern east Pacific Rise: Magnetic anomaly and bathymetric framework, *J. Geophys. Res.*, *87*(B8), 6725–6750, doi:10.1029/JB087iB08p06725.
- Langston, C. A. (1979), Structure under Mount Rainier, Washington, inferred from teleseismic body waves, *J. Geophys. Res.*, *84*(B9), 4749–4762, doi:10.1029/JB084iB09p04749.
- Laske, G., and G. Masters (1997), A global digital map of sediment thickness, *EOS Trans. AGU*, *78*(17), Spring Meet. Suppl., F483.
- Mandujano-Velazquez, J., and J. D. Keppie (2009), Middle Miocene Chiapas fold and thrust belt of Mexico: A result of collision of the Tehuantepec Transform/Ridge with the Middle America Trench, *Geol. Soc. Spec. Publ.*, *327*, 55–69.
- Manea, V. C., and M. Gurnis (2007), Subduction zone evolution and low viscosity wedges and channels, *Earth Planet. Sci. Lett.*, *264*, 22–45.
- Manea, M., and V. C. Manea (2008), On the origin of El Chichón volcano and subduction of Tehuantepec Ridge: A geodynamical perspective, *J. Volcanol. Geotherm. Res.*, *175*(4), 459–471.
- MacKenzie, L. S., G. A. Abers, S. Rondenay, and K. M. Fischer (2010), Imaging a steeply dipping subducting slab in Southern Central America, *Earth Planet. Sci. Lett.*, *296*, 459–468, doi:10.1016/j.epsl.2010.05.033.
- MASE (2007), Meso America subduction experiment, Caltech, dataset, Pasadena, CA, USA, doi:10.7909/C3RN35SP.
- Melgar, D., and X. Perez-Campos (2010), Imaging the Moho and subducted oceanic crust at the Isthmus of Tehuantepec, Mexico, from receiver functions, *Pure Appl. Geophys.*, *168*(8-9), 1449–1460.
- Nixon, G. T. (1982), The relationship between Quaternary volcanism in central Mexico and the seismicity and structure of the subducted ocean lithosphere, *Geol. Soc. Am. Bull.*, *93*, 514–523.
- Pardo, M., and G. Suárez (1995), Shape of the subducted Rivera and Cocos plates in southern Mexico: Seismic and tectonic implications, *J. Geophys. Res.*, *100*(B7), 12,357–12,373, doi:10.1029/95JB00919.
- Pearce, F. D., S. Rondenay, M. Sachpazi, M. Charalampakis, and L. H. Royden (2012), Seismic investigation of the transition from continental to oceanic subduction along the western Hellenic Subduction Zone, *J. Geophys. Res.*, doi:10.1029/2011JB009023, in press.
- Pérez-Campos, X., Y. Kim, A. Husker, P. M. Davis, R. W. Clayton, A. Iglesias, J. F. Pacheco, S. K. Singh, V. C. Manea, and M. Gurnis (2008), Horizontal subduction and truncation of the Cocos Plate beneath central Mexico, *Geophys. Res. Lett.*, *35*, L18303, doi:10.1029/2008GL035127.
- Pennington, W. D. (1981), Subduction of the eastern Panama basin and seismotectonics of northwestern South America, *J. Geophys. Res.*, *86*(B11), 10,753–10,770, doi:10.1029/JB086iB11p10753.
- Ranero, C. R., Phipps Morgan, J., Mcintosh, K., and Reichert, C. (2003), Bending-related faulting and mantle serpentinization at the Middle America trench, *Nature*, *425*, 367–373.
- Rebollar, C. J., V. H. Espindola, A. Uribe, A. Mendoza, and A. Perez-Verti (1999), Distributions of stresses and geometry of the Wadati-Benioff zone under Chiapas, Mexico, *Geofis. Int.*, *38*(2), 95–106.
- Rondenay, S. (2009), Upper mantle imaging with array recordings of converted and scattered teleseismic waves, *Surv. Geophys.*, *30*, 377–405, doi:10.1007/s10712-009-9071-5.
- Rondenay, S., M. G. Bostock, and J. Shragge (2001), Multiparameter two-dimensional inversion of scattered teleseismic body waves, 3. Application to the Cascadia 1993 data set, *J. Geophys. Res.*, *106*(B12), 30,795–30,807, doi:10.1029/2000JB000039.
- Rondenay, S., M. G. Bostock, and K. M. Fischer (2005), Multichannel inversion of scattered teleseismic body waves: Practical considerations and applicability, in *Seismic Earth: Array Analysis of Broadband Seismograms*, *Geophys. Monogr. Ser.*, vol. 157, edited by A. Levander and G. Nolet, pp. 187–203, AGU, Washington, D. C., doi:10.1029/157GM12.
- Rondenay, S., G. A. Abers, and P. E. van Keken (2008), Seismic imaging of subduction zone metamorphism, *Geology*, *36*, 275–278.
- Rondenay, S., L. G. J. Montesi, and G. A. Abers (2010), New geophysical insight into the origin of the Denali volcanic gap, *Geophys. J. Int.*, *182*, 613–630, doi: 10.1111/j.1365-246X.2010.04659.x.
- Ross, D. A., and G. G. Shor Jr. (1965), Reflection profiles across the Middle America Trench, *J. Geophys. Res.*, *70*(22), 5551–5572, doi:10.1029/JZ070i022p05551.
- Shor, G. G., and R. L. Fisher (1961), Middle America Trench: Seismic-refraction studies, *Geol. Soc. Am. Bull.*, *72*, 721–730.
- Skinner, S. M. and R. W. Clayton (2010), An evaluation of proposed mechanisms of slab flattening in central Mexico, *Pure Appl. Geophys.*, *168*, 1461–1474, doi:10.1007/s00024-010-0200-3.
- Straub, S. M., A. Gomez-Tuena, F. M. Stuart, G. F. Zellmer, R. Espinasa-Perena, Y. Cai, and Y. Iizuka (2011), Formation of hybrid arc andesites beneath thick continental crust, *Earth Planet. Sci. Lett.*, *303*, 337–347, doi:10.1016/j.epsl.2011.01.013.
- Stubailo, I., C. Begheim, and P. Davis, (2012), Structure and anisotropy of the Mexico subduction zone based on Rayleigh wave analysis and implications for the geometry of the Trans-Mexican Volcanic Belt, *J. Geophys. Res.*, *117*, B05303, doi:10.1029/2011JB008631.
- Suarez, G. (2000), Reverse faulting in the Isthmus of Tehuantepec: Backarc deformation induced by the subduction of the Tehuantepec ridge, in *Cenozoic Tectonics and Volcanism of Mexico: Geological Society of America Special Papers*, vol. 334 edited by H. Delgado-Granados, G. Aguirre-Díaz, and J. M. Stock, 263–268 p., Geol. Soc. of Am., Boulder, Colo.
- Suarez, G., and A. Lopez (2011), Crustal deformation in the southwestern Gulf of Mexico-Evidence for thrust faulting induced by the subduction of the Cocos plate, in *Simposio Dr. Zoltan de Cserna: Sesenta años Geologizando en Mexico: Distrito Federal, Mexico*, vol. 145, Instituto de Geología, UNAM.

- Suckale, J., S. Rondenay, M. Sachpazi, M. Charalampakis, A. Hosa, and L. H. Royden (2009), High-resolution seismic imaging of the western Hellenic subduction zone using teleseismic scattered waves, *Geophys. J. Int.*, *178*(2), 775–791, doi:10.1111/j.1365-246X.2009.04170.x.
- VEOX (2010), Veracruz-Oaxaca subduction experiment, Caltech, dataset, Pasadena, CA, USA, doi:10.7909/C3MW2F2C.
- Verma, S. P. (2006), Extension-related origin of magmas from a garnet bearing source in the Los Tuxtlas volcanic field, Mexico, *Int. J. Earth Sci.*, *95*(5), 871–901.
- Wada, I., and K. Wang (2009). Common depth of slab-mantle decoupling: Reconciling diversity and uniformity of subduction zones, *Geochem. Geophys. Geosyst.*, *10*, Q10009, doi:10.1029/2009GC002570.
- Waldhauser, F. and W. L. Ellsworth (2000), A double-difference earthquake location algorithm: method and application to the Northern Hayward Fault, California, *Bull. Seismol. Soc. Am.*, *90*(6), 1353–1368.
- Woodcock, S. (1975), Crustal structure of the Tehuantepec ridge and adjacent continental margins of southwestern Mexico and western Guatemala, MS thesis, Oreg. State Univ., Corvallis, OR, USA.